Field emission enhancement in nitrogen-ion-implanted ultrananocrystalline diamond films

P. T. Joseph,[1] N. H. Tai,[1] Chi-Young Lee,[2] H. Niu,[3] W. F. Pong,[4] and I. N. Lin[4,a)]
[1]*Department of Materials Science and Engineering, National Tsing Hua University, Hsin-Chu, Taiwan 300, Republic of China*
[2]*Materials Science Center, National Tsing Hua University, Hsin-Chu, Taiwan 300, Republic of China*
[3]*Nuclear Science and Technology, Development Center Accelerator Division, National Tsing Hua University, Hsin-Chu, Taiwan 300, Republic of China*
[4]*Department of Physics, Tamkang University, Tamsui, Taiwan 251, Republic of China*

(Received 17 September 2007; accepted 24 December 2007; published online 29 February 2008)

Enhanced electron field emission (EFE) properties for ultrananocrystalline diamond (UNCD) films grown on silicon substrate were achieved, especially due to the high dose N ion implantation. Secondary ion mass spectroscopy, Raman spectroscopy, and x-ray photoelectron spectroscopy measurements indicated that the N ion implantation first expelled H^-, induced the formation of disordered carbon (or defect complex), and then induced the amorphous phase, as the ion implantation dose increased. The postimplantation annealing process healed the atomic defects, but converted the disordered carbon to a stable defect complex, and amorphous carbon into a more stable graphitic phase. The EFE characteristics of the high dose ($>10^{15}$ ions/cm^2) ion-implanted UNCD were maintained at an enhanced level, whereas those of the low dose ($<10^{14}$ ions/cm^2) ion-implanted ones were reverted to the original values after the annealing process. Ion implantation over a critical dose (1×10^{15} ions/cm^2) was required to improve the EFE properties of UNCD films. © *2008 American Institute of Physics*. [DOI: 10.1063/1.2885348]

I. INTRODUCTION

Field emission from carbon and related materials has received great attention due to the strong potential of this material to be employed as a cold cathode material in flat panel displays and other electron emitting devices.[1–3] Diamond can outperform the traditional field emitters with high work function materials such as tungsten, molybdenum, or silicon tips due to its superior electron field emission (EFE) distinctiveness in addition to mechanical permanence and chemical inertness. Ultrananocrystalline diamond (UNCD) films are advanced among the carbon family with 2–5 nm sized grains and 0.3–0.4 nm wide grain boundaries since the abundance of the grain boundaries facilitates the electron conduction.[4] The great promise that a diamond or an UNCD film bears as a material for the fabrication of cold cathode or other electron emitting devices requires the film to be conductive. Presumably, nitrogen doping at the substitutional sites in diamond can act as electron donors.[5–7] However the efforts to improve field emission by incorporating N into conventional diamond with micron sized grains has been reported to be unsuccessful due to the formation of deep donors in materials.[8]

In contrast, incorporation of N into diamond films with nanosized grains has been shown to enhance its field emission properties,[9,10] which was ascribed to the phenomenon that the N incorporates into the grain boundaries, and enhances its conductivity.[10,11] However, the dopant concentration is limited when the N doped into UNCD by incorporating N species in the microwave induced plasma. Another technique that can incorporate high concentration of N into UNCD is needed. Moreover, ion irradiation induced enhancement in the field emission properties of diamond[12,13] and carbon fibers[14–16] have been reported, which was attributed to the inducing of defects. However, postannealing could revert the enhanced EFE properties to the original level due to the removal of defects.[12] Therefore, an other approach, which can preserve the enhanced EFE properties even after the annealing, is called for.

In this article, we report the effects of 100 keV N ion implantation into UNCD films on their field emission properties. We have also investigated how the ion-implantation effect on UNCD was different from that for conventional diamond films. A detailed study has been carried out to reveal the structural and chemical states of the UNCD films before implantation, as implanted, and after annealing by using secondary ion mass spectroscopy (SIMS), Raman spectroscopy, and x-ray photoelectron spectroscopy (XPS). The results were evaluated in terms of their effect on the enhancement of the UNCD field emission properties. From our results, it was found that N ion implantation with doses above critical dose enhanced the field emission properties, which were preserved even after the annealing process.

II. EXPERIMENTAL DETAILS

The UNCD films with ultrasmooth surface characteristics at the nanoscale were prepared for the ion implantation. The UNCD films were grown on an *n*-type silicon substrate using a microwave plasma-enhanced chemical vapor deposition (MPECVD) process (IPLAS-Cyrannus). Prior to the

a)Electronic mail: inanlin@mail.tku.edu.tw.

growth of UNCD films, the substrate was preseeded by carburization in hydrocarbon plasma containing 1% CH_4/Ar at 1200 W and at 150 Torr for 25 min followed by ultrasonication in nanodiamond powder containing methanol for 30 min. The deposition of UNCD on substrates was carried out in a CH_4/Ar plasma with the same parameters as those of the hydrocarbon plasma pretreatment. The growth process was carried out at low temperatures (<465 °C) without heating the substrate for 180 min to reach a thickness of 250 nm, which was confirmed from the cross-sectional field emission scanning electron microscopy (FESEM) (Joel 6500) image (figure not shown). The UNCD films were implanted to a dose of $10^{11}-10^{16}$ ions/cm^2 at room temperature and at 5×10^{-6} Torr with N of 100 keV (HVEE500KV-Implantor) kinetic energy. The TRIM computer code[17] was used to estimate the trajectory of N ions in UNCD films. After implantation, the samples were annealed at 600 °C for 1 h in $H_2(10\%)/N_2$ medium to heal the damage resulted by ion implantation. The analyses were performed using SIMS (Cameca, IMS-4f), Raman spectroscopy (Renishaw), and XPS (PHI, 1600). Room temperature field emission properties of the samples were measured with an electrometer (Keithley 237) using a parallel cathode-anode setup,[18] and the Fowler–Nordheim (FN) model[19] was used to explain the EFE behavior of materials.

III. RESULTS AND DISCUSSION

Figure 1 shows the field emission properties of UNCD films implanted with different doses of N ions, before and after the annealing process, where the lines show the theoretical fit to the experimental data. The insets of Figs. 1(a) and 1(b) show the FN plot, $\ln(J/E^2)$ versus $1/E$, of the corresponding field emission data. The turn-on field designated here is the lowest value of the FN plot, corresponding to the intersection of the segments. The variation in E_0 value with different ion implantation doses, which is derived from Fig. 1(a), is plotted in Fig. 2. This figure indicates that a decrease in the turn-on field is significant (open squares) due to N ion implantation. The turn-on field decreases from $(E_0)_{00}=9.2$ V/μm for the pristine UNCD film to $(E_0)_{11}=5.5$ V/μm for the UNCD film implanted with a dose of 10^{11} ions/cm^2 (N_{11} samples). The E_0 value increases with N ion dose and for the UNCD film implanted with 10^{16} ions/cm^2 (N_{16} samples), $(E_0)_{16}$ is approximately equal to 8.8 V/μm. The turn-on field for inducing the EFE process is increased due to postannealing, except for N_{16} sample. The E_0 value of sample N_{16}, $(E_0)_{16}$, decreases further from 8.8 to 7.0 V/μm due to postannealing at 600 °C, which is shown as solid circles in Fig. 2(a).

Figure 1(a) shows that the increase in EFE current density due to N ion implantation does not correlate very well with the N ion dosage. A very high current density, $(J_e)_{16}=8.2$ mA/cm^2, at an applied field of 20 V/μm, is achieved for N_{16} samples as compared to $(J_e)_{00}=1.6$ mA/cm^2 for the pristine UNCD film at the same field. The electron emission current density corresponding to a 20 V/μm applied field of the samples after ion implantation/postannealing is shown in Fig. 2(b). It indicates that the postannealing reverted the EFE

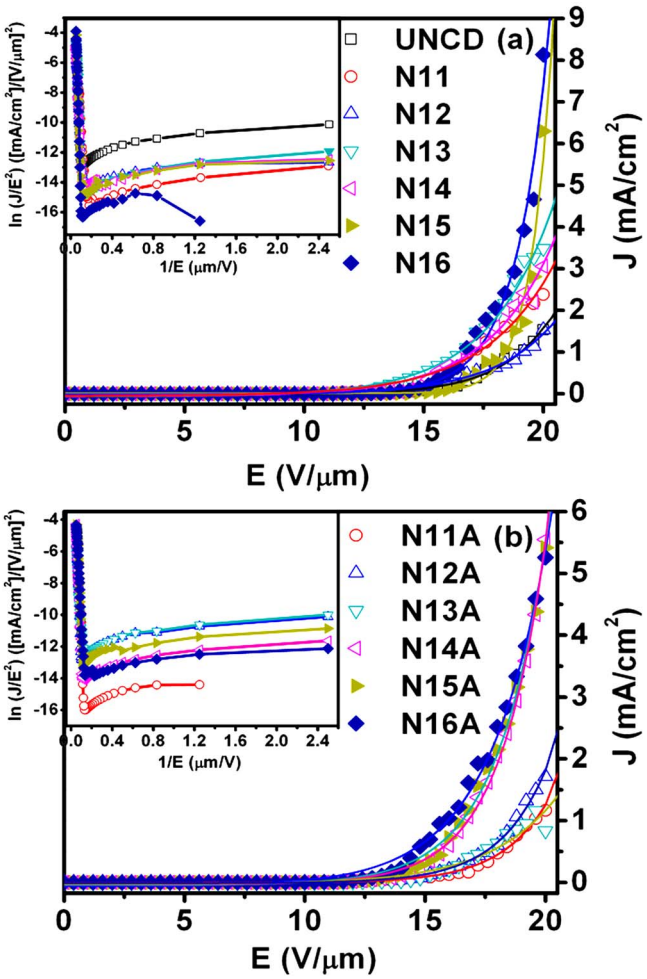

FIG. 1. (Color online) EFE property of UNCD films (a) before and after N ion implantation and (b) after postannealing. The insets show the FN plot, and the lines are the theoretical fit of the FN model. The open square symbols in (a) are pristine UNCD, whereas the ion-implanted samples designated as $N_{11}-N_{16}$ (before annealing) and $N_{11A}-N_{16A}$ (after postimplantation annealing) are given with respect to the dosages from 1×10^{11} to 1×10^{16} ions/cm^2. The postannealing is carried out at 600 °C in $H_2(10\%)/N_2$ for 1 h.

current density back to a level the same as that of pristine UNCD for the low dose (<10^{13} ions/cm^2) ion-implanted UNCD films. Nevertheless, the high emission current densities for the high dose (10^{14} ions/cm^2 or above) N-ion implanted samples are retained. The J_e increased from 1.6 to 5.2 mA/cm^2 and E_0 decreased from 9.2 to 7.0 V/μm for N_{16} samples, which were subjected to 10^{16} ions/cm^2 N ion implantation and postannealing at 600 °C. Based on the findings, it is evident that ion implantation over a critical dose is required to improve the EFE properties of UNCD films.

To explain the basis of enhancement in the field emission properties, we have carried out detailed investigations using SIMS, Raman spectroscopy, and XPS. It should be noted that in SIMS investigation, since a direct observation of secondary N ions is difficult due to the interference of hydrocarbon masses for positive N and lack of stable negative N, the CN depth profile of 26.003 amu (negative polarity mode) is used to monitor the presence of nitrogen in UNCD films.[9,20] Specifically, for investigating the origin of enhanced field emis-

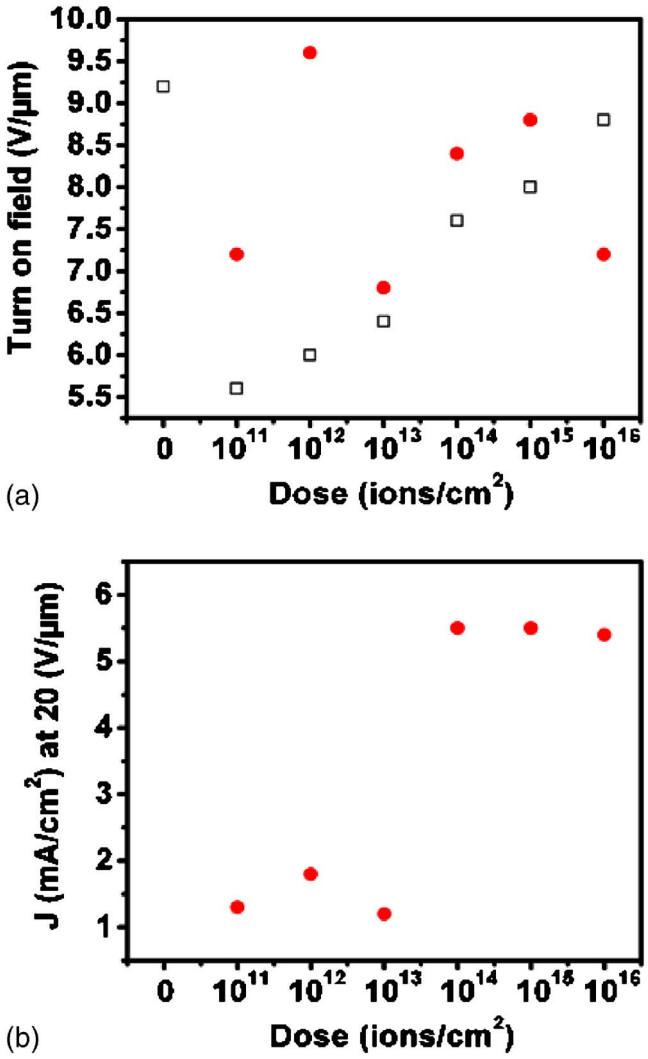

FIG. 2. (Color online) (a) The turn-on field (E_0) variation with N-ion implantation dosages, before (open squares) and after (closed circles) annealing, and (b) the EFE current density (J_e) at 20 V/μm applied field variation with N ion implantation dosages (after annealing).

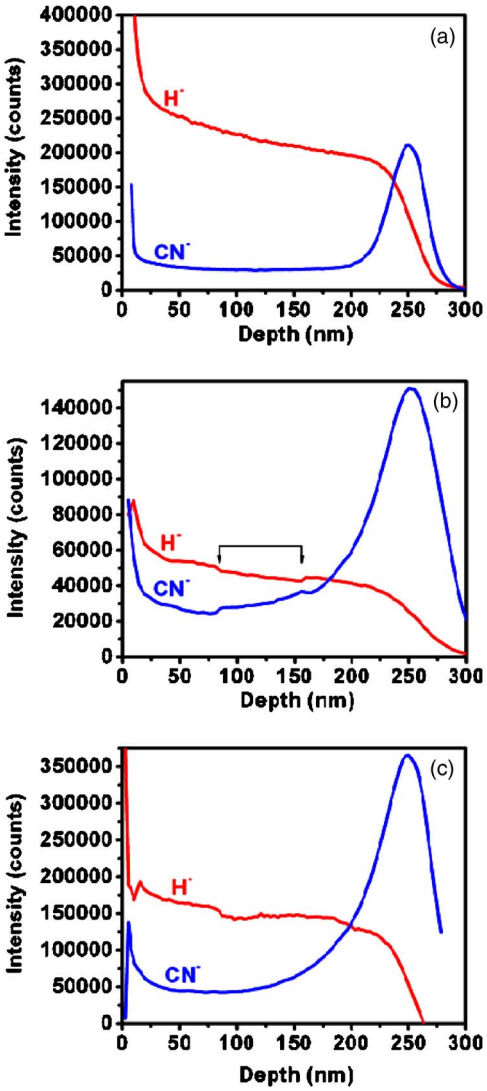

FIG. 3. (Color online) SIMS depth profile obtained in the negative polarity mode for (a) pristine UNCD films, (b) after N-ion implantation with a dosage of 10^{16} ions/cm^2, and (c) after postannealing at 600 °C in $H_2(10\%)/N_2$ for 1 h.

sion, we have compared the SIMS depth profiles of pristine and high dosage ion-implanted UNCD samples (N_{16}). The depth profile of H^- and CN^- intensities of the pristine UNCD film is shown in Fig. 3(a). The H^- content in the pristine UNCD film is slightly increased with growth time toward the surface. The CN^- is dominant at the interface between the UNCD and Si substrate, which is attributed to the presence of N, which is adsorbed from the environment in the initial growth phase. The depth profile [Fig. 3(b)] indicates that implanting of UNCD films (N_{16}) with a high dose of N ions (10^{16} ions/cm^2) results in the formation of steps of H^- and CN^- in the middle region (80–160 nm) (indicated by arrows). The H^- intensity profile, when compared to that of pristine UNCD, shows a drastic decrease in H^- content from 250,000 counts (average) to 60,000 counts (average), due to ion implantation.

The approximate penetration depth of the implanted N ions estimated from TRIM code calculation is around 85–155 nm, which is in agreement with the CN^- steps observed in the SIMS depth profile. The nuclear energy loss is dominating at the end of the trajectory of irradiating ions causing lattice damage or displacement of atoms in that region. The presence of CN^- and H^- steps in a SIMS depth profile can evidently be ascribed to the nuclear energy loss of implanted ions, which displaces the carbon ions. These SIMS observations indicate the expulsion of H due to N ion implantation. The SIMS depth profiles of a postannealed UNCD film in Fig. 3(c) show the disappearance of CN^- and H^- steps due to diffusion of the ions. The N ions implanted are presumed to be distributed uniformly in the UNCD films after postannealing. The intake of H back to the UNCD film due to annealing is also evident (the H^- ion counts increase from 60,000 (average) for as-implanted samples to 150,000 counts (average) for annealed ones).

The Raman spectroscopic measurements were performed at room temperature using a 632.8 nm laser as the excitation source. Figure 4(a) shows the Raman spectra of a pristine UNCD film. A broadened diamond peak is generally observed for the UNCD films due to the smallness in grain size (approximately nanometer scale) and also due to the increasing concentration of a variety of growth defects in-

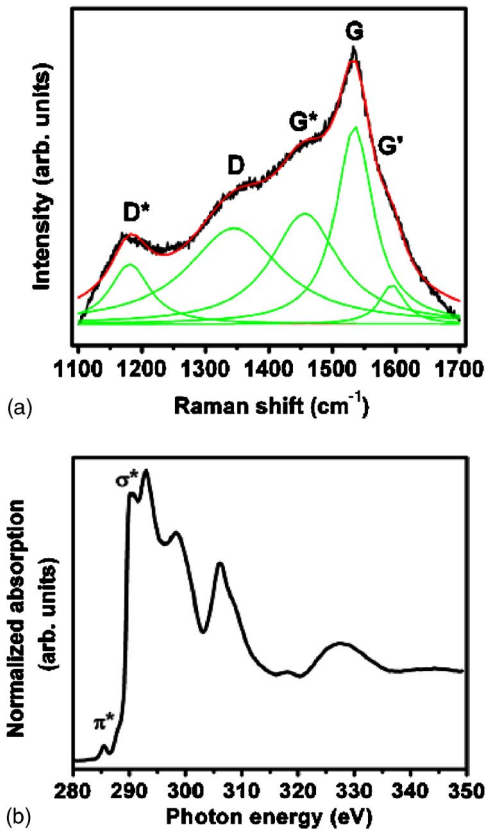

FIG. 4. (Color online) (a) Raman spectra and (b) NEXAFS spectra of the pristine UNCD film.

cluding point defects, twins, internal stresses and sp^2 admixtures.[21] The peaks at about 1150 and 1450 cm^{-1} are affirmed to *trans*-polyacetylene (D^* and G^* band) present on the surface and grain boundaries of UNCD films.[22] Contrary to the Raman peak at 1332 cm^{-1} for conventional diamond films, a broad peak observed at about 1350 cm^{-1} is assigned as a D band, and that observed at about 1532 cm^{-1} is assigned as a G band for UNCD and NCD films. The detailed features of UNCD explained by different reports are in good agreement with the obtained data.[18,22] To confirm unambiguously the sp^3-bond nature of the films, near edge x-ray absorption fine structure (NEXAFS) spectra of the films are necessary, as Raman spectra are not able to indicate that the grains in UNCD films are that of diamond (sp^3 bonded). The sharp rise in absorption near 289.7 eV and a deep valley near 302.5 eV (labeled as σ^* band) in the typical NEXAFS spectra shown in Fig. 4(b) clearly indicates that the UNCD films are diamond films. Moreover, a small peak at 285.0 eV (labeled as a π^* band) indicates that the films contain a small proportion of graphitic phase.

Implantation with N ions below the critical dose (10^{14} ions/cm^2) did not collapse the UNCD structure, and all the corresponding Raman spectra resemble those shown in Fig. 4(a). Figure 5(a) reveals that the D band around 1350 cm^{-1} is more noticeable for N_{14} samples in this implantation dose, which is a clear indication of the increased defects due to ion implantation.[16,23] The postannealing did not change the Raman spectra of these films (not shown). Figure 5(b) illustrates the amorphization induced in the UNCD film

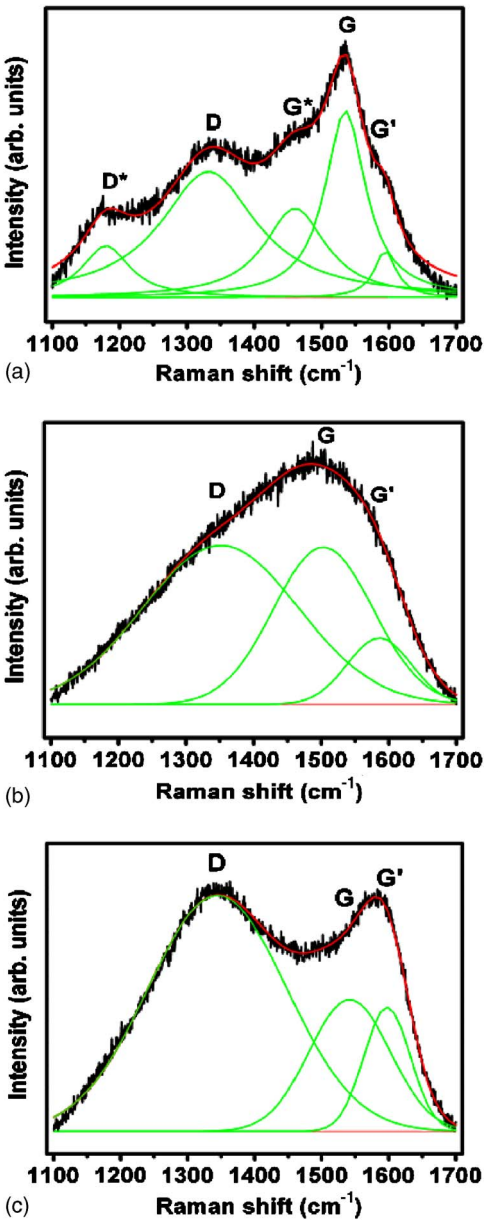

FIG. 5. (Color online) Raman spectra of the UNCD film (a) for N-ion-implanted with dosages of 10^{14} ions/cm^2, (b) for N-ion-implanted with dosages of 10^{16} ions/cm^2, and (c) for N-ion-implanted with dosages of 10^{16} ions/cm^2 and postannealing at 600 °C in $H_2(10\%)/N_2$ for 1 h.

implanted with a dose of 10^{16} N ions/cm^2. The surface amorphization induced by implantation is transformed to a graphitic phase due to the postannealing process [Fig. 5(c)]. Such a phenomenon is in accord with literature reports.[5,26] Additionally, transparent property studies carried out with a UV-vis-near infrared spectrophotometer for high dose (10^{16} ions/cm^2) N-ion-implanted UNCD grown on quartz substrate shows a reduction in the transmittance, which is further evidence of the disordered sp^2 formation (figure not shown). The postannealing further reduced the transparency of the UNCD film, which supports the Raman data for the formation of a graphitic structure. It should be noted that the critical dose for the formation of a graphitic phase found from our results is 10^{15} ions/cm^2 or above, and the presence of a graphitic phase after ion implantation and postannealing is also observed for N_{15} samples, but to a much lesser extent.

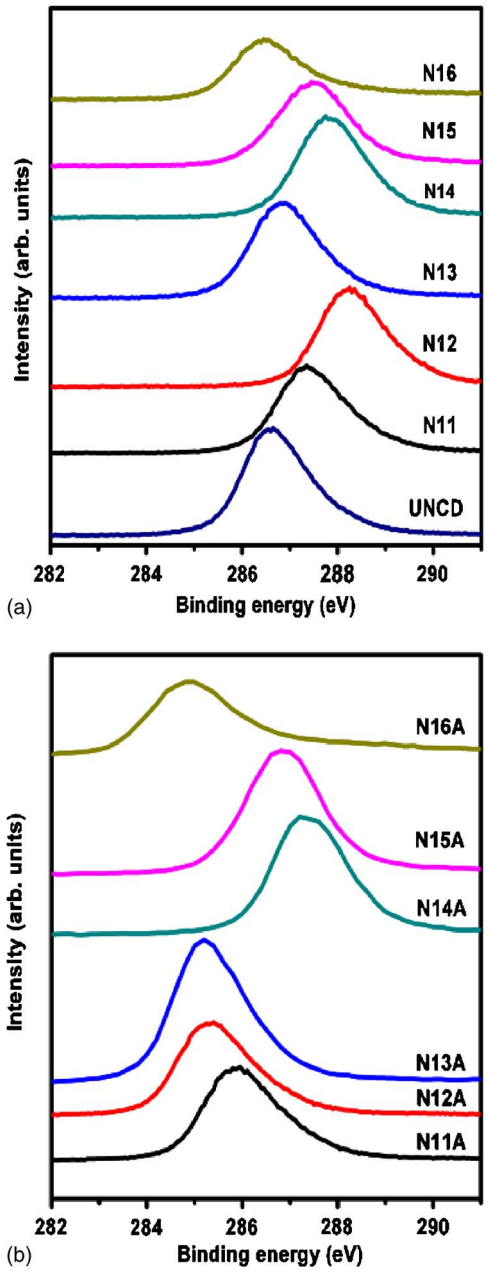

FIG. 6. (Color online) XPS C1*s* peak positions of the UNCD films (a) before and after N ion implantation and (b) after postannealing. The ion-implanted samples were designated as N_{11}–N_{16} (before annealing) and N_{11A}–N_{16A} (after postimplantation annealing), with respect to the dosages from 1×10^{11} to 1×10^{16} ions/cm^2. The postannealing was carried out at 600 °C in $H_2(10\%)/N_2$ for 1 h.

While the modification on the structure of UNCD films due to ion implantation and postannealing inferred by Raman spectroscopy can be correlated with the change in EFE properties of the films, modification of surface properties is known to even more pronouncedly influence the EFE properties of the materials.[6,12] Therefore, to understand how the ion implantation/postannealing processes modified the surface characteristics of the UNCD films, XPS studies are carried out at a pressure of $<10^{-9}$ Torr. The carbon 1*s* core level (C1*s*) peak of pristine and N-ion-implanted UNCD films obtained from the XPS are shown in Fig. 6(a). The C1*s* peak of the UNCD sample is observed at 286.65 eV, which is shifted by 1.05 eV higher than the normal C1*s* peak[15] (the blueshift), and is possibly due to the surface charging or oxidation of UNCD, which implies the existence of electron trapping centers in these films.[24,25] We have not found any significant N1*s* peak from the ion-implanted UNCD films during the measurement. This is probably due to the large penetration depth of implanted ions, such that the N is residing inside the films at a level far below the sensitivity of the XPS measurement.

The increase in ion implantation dose results in a larger C1*s* peak shift (N_{11} and N_{12} samples). The additional blueshift is probably due to the removal of H^- (which is also evident from the SIMS depth profile). The H ions are presumed to be absorbed in atomic defects (vacancies), compensating for dangling bonds.[4] Removal of H^- exposes the dangling bonds, which act as trapping centers for electrons. Trapping of charges in the defect states is the probable reason for the increase in surface charging and the additional C1*s* blueshift after ion implantation.[24,25] In contrast, the C1*s* peak shifts in the reverse direction to lower the binding energies, suggesting the onset of formation of disordered carbon at an implantation dose of 10^{13} ions/cm^2 (N_{13} sample). The presence of disordered carbon eliminates the atomic defects (the electron trapping centers), reducing the surface charge. A further increase in the dose to 10^{14} ions/cm^2 produces more defects, which leads to the formation of defect complexes (carbon clusters, vacancy dimers, trimers, etc.). These defect complexes also behave as electron traps and further enhance the surface charging, leading to a blueshift of the C1*s* peak for the N_{14} sample. The C1*s* peak shifts to lower binding energies at a higher implantation dose (10^{15} ions/cm^2, N_{15}), indicating the lowering of the surface resistivity, probably via the formation of amorphous carbon and nano-sp^2 clusters. Such a phenomenon is in agreement with the observed amorphization for Raman spectra [Fig. 5(b)].[24] For the N_{16} sample, the C1*s* peak reverse shifts further, presumably due to the formation of a larger proportion of amorphous carbons and nano-sp^2 clusters. These phenomena are analogous to the implantation dose dependency of conductivity in a conventional crystalline diamond.[26]

After annealing, the C1*s* peaks reversely shift toward the normal C1*s* peak, at 284.5 eV, for all the dosages [Fig. 6(b)] as compared to the as-implanted samples, except for N_{14A} and N_{15A} samples with a dose of 10^{14} or 10^{15} ions/cm^2, in which the C1*s* peak remains at a higher binding energy. The reverse shifting of the C1*s* peak for the low dose ion-implanted samples (N_{11A}–N_{13A}) is accounted for by the compensation of the defects by the intake of H due to annealing.[5] Regarding N_{14A} and N_{15A} samples, the formed defect complexes are stable against the annealing process, leading to unchanged XPS spectra. For the samples implanted with the highest dose (10^{16} ions/cm^2, N_{16A}), the UNCD surface structure collapsed to nanographite (sp^2). The surface charges are eliminated such that the C1*s* peaks reverse shift toward the normal C1*s* peak of 285 eV. The formation of nanographites is also confirmed by the Raman studies [Fig. 5(c)].

The effects of ion implantation on UNCD are briefly summarized in Table I. At low doses ($<10^{13}$ ion/cm^2), the H

TABLE I. Effects of ion implantation and postimplantation annealing processes on the formation of defects in UNCD.

Dose	As implantation	Implantation and annealing	Defects in materials
$10^{11}-10^{12}$	H^- removal	H^- intake	Lightly doped N
10^{13}	Displaced carbon	Healed	Lightly doped N
10^{14}	Defect complex (carbon clusters, vacancy dimer, trimer, etc.)	Stabilized to carbon clusters	Carbon clusters+doped N and grain boundary N
10^{15}	Defect complex (with a small proportion of amorphous)	Carbon clusters+ nanographites (small concentration)	Carbon clusters+ nanographites (small concentration) + doped N and grain boundary N
10^{16}	amorphous (large concentration)	Nanographites (large concentration)	Nanographites (large concentration) + doped N and grain boundary N

removal and onset of the formation of disordered carbon occur. The defects induced can be healed, in addition to the intake of H, by a postimplantation annealing process. At a medium dose ($10^{14}-10^{15}$ ion/cm^2), defect complexes (carbon clusters, vacancy dimers, trimers, etc.) are induced, which form stabilized defects (carbon clusters) after annealing. Amorphization is induced at high dose ion implantation (10^{16} ion/cm^2), which is converted into nanographites after the annealing process.

Although the defect formation mechanism summarized in Table I is proposed based on the XPS observation, which is a surface sensitive investigation, these defects are presumed to be induced throughout the depth of the UNCD films, where the energetic ions passed through. The kinetics of defect formation due to ion implantation can account for the modification of the EFE behavior of UNCD films. Interband electronic states in diamond materials are formed due to the presence of small defects, which facilitate the jump of electrons from valence band to conduction band and lower the turn-on field (E_0) for the EFE process. Such a mechanism applies when the defects are small in size, which occurs for the low dose as-implanted samples ($N_{11}-N_{13}$) [Fig. 2(a), open squares]. After annealing, the defects are either annihilated or collapsed to form a defect complex and thereafter eliminate the intermediate energy levels. The turn-on field (E_0) is thus brought back to the original high level [Fig. 2(a), closed circles]. However, for the N_{16} samples, ion implantation/postannealing induces the formation of nanographite, which facilitates the electron transport and leads to a further lowering of the turn-on field (E_0), but to a much lesser extent. Restated, the modification of the characteristics of defects induced due to the ion implantation and annealing process is the prime factor altering the turn-on field (E_0) for UNCD.

The variation of EFE current density (J_e) of ion-implanted/postannealed samples with the dose changes differently from that of the turn-on field (E_0). First of all, most of the N ions implanted are expected to reside in the grain boundary region for the N_{16} sample. The argument, based on the SIMS profile in Fig. 3(b), is that the N ions implanted (10^{16} ions/cm^2) are residing in a region from 85–155 nm underneath the surface. The estimated N ion density is 1.3×10^{23} cm^{-3}, and the induced stresses will be higher if all the implanted N ions are incorporated into the diamond grains, which prohibits the substitutional replacement of all N in the diamond lattice. This is especially true if we take into account the extremely small diamond grain size (~5 nm) in the UNCD film.

Literature reports[10,11] indicate that growing UNCD by using plasma containing high N_2 concentration (CH_4/Ar–20% N_2) results in the incorporation of N in grain boundaries and forms a conducting grain boundary layer. Such conducting grain boundaries facilitate the electron transport, dramatically reducing the resistivity of the films and increasing the EFE current density (J_e). It is believed that the same mechanism is applicable in our case. For N_{16} samples, the dosage of N is high enough to induce the formation of grain boundary doping of N species. Each N replacing a C in the grain boundary can inject one electron into the UNCD lattice, converting the materials into a semiconductor. The presence of grain boundary N species can therefore markedly enhance the EFE process. The same mechanism can be applied in explaining the improvement in the EFE properties of N_{14} and N_{15} samples due to ion implantation/postannealing. The dosage of 10^{14} ions/cm^2 seems to be the critical dosage to induce a grain boundary doping of nitrogen. It should be noted that the N concentration for ion-implanted UNCD films after annealing is estimated to be about 0.4×10^{23} cm^{-3} for N_{16} samples (assuming that the N ions implanted diffuse away and distribute uniformly in the UNCD films). Such a doping level is markedly higher than the nitrogen concentration reached when N is incorporated in UNCD via the MPECVD process.[11,20]

IV. CONCLUSIONS

The N-ion-implanted UNCD films with a modified structure and better EFE properties are demonstrated in this work. The N-ion implantation first expels the H^- and leads to the formation of a disordered carbon and a defect complex, and then transformed the diamond into an amorphous form at increased ion implantation doses. Postannealing heals the atomic defects and converts the disordered carbon to a stable defect complex and the amorphous carbon into a more stable graphitic phase. The modification on the EFE properties of the films due to ion implantation/postannealing is closely

related to the nature of defects induced. Ion implantation over a critical dose (1×10^{15} ions/cm^2) is required to improve the EFE properties of UNCD films. A high EFE current density of 5.5 mA/cm^2 is achieved at an applied field of 20 V/μm for UNCD films implanted with N ion doses above 10^{14} ions/cm^2 and postannealed.

ACKNOWLEDGMENTS

The authors would like to thank the National Science Council, Republic of China for the support of this research through the Project No. NSC 96-2112-M032-011-MY3.

[1]W. Zhu, G. P. Kochanski, and S. Jin, Science **282**, 1471 (1998).
[2]K. Okano, K. Hoshina, M. Iida, S. Koizumi, and T. Inuzuka, Appl. Phys. Lett. **64**, 2742 (1994).
[3]W. L. Wang, J. D. Fabbri, T. M. Willey, J. R. I. Lee, J. E. Dahl, R. M. K. Carlson, P. R. Schreiner, A. A. Fokin, B. A. Tkachenko, N. A. Fokina, W. Meevasana, N. Mannella, K. Tanaka, X. J. Zhou, T. van Buuren, M. A. Kelly, Z. Hussain, N. A. Melosh, and Z.-X. Shen, Science **316**, 1460 (2007).
[4]D. Zhou, T. G. McCauley, L. C. Qin, A. R. Krauss, and D. M. Gruen, J. Appl. Phys. **83**, 540 (1998).
[5]R. Kailash, Carbon **37**, 781 (1999).
[6]W. Zhu, G. P. Kochanski, S. Jin, and L. Seibles, J. Appl. Phys. **78**, 2707 (1995).
[7]S. A. Kajihara, A. Antonelli, and J. Bernholc, Phys. Rev. Lett. **66**, 2010 (1991).
[8]E. Rohrer, C. F. O. Graeff, R. Janssen, C. E. Nebel, H. Guettler, and R. Zachai, Phys. Rev. B **54**, 7874 (1996).
[9]D. Zhou, A. R. Krauss, L. C. Qin, T. G. McCauley, D. M. Gruen, T. D. Corrigan, and R. P. H. Chang, J. Appl. Phys. **82**, 4546 (1997).
[10]T. D. Corrigan, D. M. Gruen, A. R. Krauss, P. Zapol, and R. P. H. Chang, Diamond Relat. Mater. **11**, 43 (2002).
[11]S. Bhattacharyya, O. Auciello, J. Birrell, J. A. Carlisle, L. A. Curtiss, A. N. Goyette, D. M. Gruen, A. R. Krauss, J. Schlueter, A. Sumant, and P. Zapol, Appl. Phys. Lett. **79**, 1441 (2001).
[12]W. Zhu, G. P. Kochanski, S. Jin, L. Seibles, D. C. Jacobson, M. McCormack, and A. E. White, Appl. Phys. Lett. **67**, 1157 (1995).
[13]P. M. Koinkar, R. S. Khairnar, S. A. Khan, R. P. Gupta, D. K. Avasthi, and M. A. More, Nucl. Instrum. Methods Phys. Res. B **244**, 217 (2006).
[14]K. C. Walter, H. H. Kung, and C. J. Maggiore, Appl. Phys. Lett. **71**, 1320 (1997).
[15]S. Talapatra, P. G. Ganesan, T. Kim, R. Vajtai, M. Huang, M. Shima, G. Ramanath, D. Srivastava, S. C. Deevi, and P. M. Ajayan, Phys. Rev. Lett. **95**, 097201 (2005).
[16]S. Talapatra, J. Y. Cheng, N. Chakrapani, S. Trasobares, A. Cao, R. Vajtai, M. B. Huang, and P. M. Ajayan, Nanotechnology **17**, 305 (2006).
[17]J. F. Zielger, J. P. Biersack, and U. Littmark, *The Stopping and Range of Ions in Solids* (Pergamon, New York, 1985).
[18]Y. C. Lee, S. J. Lin, I. N. Lin, and H. F. Cheng, J. Appl. Phys. **97**, 054310 (2005).
[19]R. H. Fowler and L. Nordheim, Proc. R. Soc. London, Ser. A **119**, 173 (1928).
[20]D. Zhou, F. A. Stevie, L. Chow, J. McKinley, H. Gnaser, and V. H. Desai, J. Vac. Sci. Technol. A **17**, 1135 (1999).
[21]A. Ilie, A. C. Ferrari, T. Yagi, S. E. Rodil, J. Robertson, E. Barborini, and P. Milani, J. Appl. Phys. **90**, 2024 (2001).
[22]A. C. Ferrari and J. Robertson, Phys. Rev. B **63**, 121405 (2001).
[23]K. Fabisiak, M. Maar-Stumm, and E. Blank, Diamond Relat. Mater. **2**, 722 (1993).
[24]Y. Fan, A. G. Fitzgerald, P. John, C. E. Troupe, and J. I. B. Wilson, Surf. Interface Anal. **34**, 703 (2002).
[25]A. Hoffman, I. Andrienko, D. N. Jamieson, and S. Pawar, Appl. Phys. Lett. **86**, 044103 (2005).
[26]S. Prawer and R. Kalish, Phys. Rev. B **51**, 15711 (1995).